Effects of Sample Width and Sidewalls on Downward Flame Spread over XPS Slabs

WEIGUANG An[a,b], HUAHUA XIAO[a], JINHUA SUN[a], K.M. LIEW[b], WEIGANG YAN[a], YANG ZHOU[a], LIN JIANG[a], XINJIE HUANG[c]
[a]Sate Key Laboratory of Fire Science, University of Science and Technology of China
[b]Department of Civil and Architectural Engineering, City University of Hong Kong
[c]School of Civil Engineering and Architecture, Anhui University of Technology
[a]Hefei, Anhui, 230026, PR China
[b]Kowloon, Hong Kong, 999077, PR China
[c]Ma'anshan, Anhui, 243002, PR China

ABSTRACT

To study the effects of sample width and sidewalls on downward flame spread over extruded polystyrene (XPS) slabs, a series of laboratory-scale experiments were conducted. Flame shape, flame spread rate, mass loss rate and temperature were recorded. For XPS without sidewalls, the average maximum flame height (H) and average flame area per unit of width (A/w) rise linearly with an increase in sample width (w) and mass loss rate per unit of width. When sidewalls are absent, flame spread rate first drops and then rises with an increase in width. This trend is determined by gas-phase heat transfer. When sidewalls are present, flame spread rate increases with a rise in width, and solid-phase heat conduction determines the trend. Sidewall effects are comprised of four aspects: oxygen concentration near the sidewalls and gypsum board is low, which leads to reduced flame heat flux; upward and front air flow is intensified; the flame is stretched, and the surface flame is weakened; and molten XPS mass decreases. For narrow samples, H and A/w with sidewalls are higher than those without sidewalls, while the reverse was observed in wider samples. The mass loss rate, preheating length and average flame spread rate with sidewalls are smaller than those obtained without sidewalls. Flame spread acceleration with sidewalls occurs at a broader width than that without sidewalls. The experimental results agree well with the theoretical analysis.

KEYWORDS: flame spread, extruded polystyrene (XPS), width effects, sidewall effects

NOMENCLATURE LISTING

A_1	flame area (cm^2)	T_f	flame temperature (K)
A_2	preheating zone area (cm^2)	T_∞	ambient temperature (K)
A_c	sample cross section area (cm^2)	T_m	solid-phase temperature (K)
A	average flame area (cm^2)	u_0	initial velocity of gaseous fuel (cm/s)
c_p	specific heat (J/g K)	v_p	predicted flame spread rate (cm/s)
D_e	effective diffusivity	v_f	measured average flame spread rate (cm/s)
F_{12}	view factor of flame to unburned XPS	w	sample width (cm)
g	acceleration of gravity (m/s^2)	W	burning width (cm)
H	average maximum flame height (cm)	x_0	position where temperature begins to rise(cm)
H_{max}	maximum flame height (cm)	Y	flame spread distance (cm)
h_c	combustion heat (J/g)		
m	instantaneous XPS mass (g)	**Greek**	
m_0	initial XPS mass (g)	ρ_∞	density of ambient gas(g/cm^3)
$\dot{m}$	mass loss rate (g/s)	ρ	sample density (g/cm^3)
$\dot{m}_1$	mass growth rate of molten XPS (g/s)	δ_{ph}	preheating length (cm)
$\dot{q}''_{cond}$	heat flux in solid (W/m^2)	λ_m	thermal conductivity of molten XPS(W/cm K)
$\dot{q}''_g$	gas-phase heat flux(W/m^2)	ε_f	flame emissivity
T_{ig}	ignition temperature (K)	σ	Stefan-Boltzmann constant
T_s	surface temperature (K)	θ	flame angle

INTRODUCTION

Insulation materials are widely employed in building facades to save energy in China. XPS (extruded polystyrene) foam is a typical insulation material with good properties, such as excellent heat-shielding performance, light weight and higher corrosion resistance. However, the fire risk of XPS should not be ignored, since it can be easily ignited and the resulting flame spread rate is high. In addition, the combustion of XPS usually releases considerable heat and toxic gas. A good example is the fire which occurred on the facade of the Beijing Television Central Culture (TVCC) building in February 2009. The fire began on the top of the building, whose facade was covered with XPS foam. Then it quickly spread downward through the entire building, causing considerable loss. Furthermore, building facades are becoming increasingly complex, and U-shaped structures are typical. The U-shaped structure describes the concave building facade, which has two sidewalls vertical to another wall (Fig. 1(a)). The sidewalls of U-shaped structures significantly affect facade fires (Fig. 1(b)).

(a) (b)

Fig. 1. (a) U-shaped facade structure; (b) a facade fire in a tall building with a U-shaped facade structure.

More attention has recently been given to the fire safety of XPS material. The characteristics of horizontal flame spread over XPS surface were studied by Zhang et al. [1]. They conducted experiments on a plateau (Lhasa, China), where the atmospheric pressure is lower than that at sea level, to explore the environmental effects (especially the pressure effect) on XPS flame spread. They suggested that the temperature rise process in the solid phase is comprised of three stages, and that flame spread rate is lower at higher elevations. Huang et al. [2] investigated flame spread characteristics of XPS in different environments. They predicted the scope of XPS flame spread rate and concluded that pool fire length constantly increases as the fire spreads. Although little research concerning the width effect on XPS flame spread is available, a considerable body of research concerning other materials is available in the literature. For horizontal flame spread, Li et al. [3] demonstrated that flame spread rate increased with a rise in sample width, while Mell et al. [4] concluded that the reverse is true. Rangwala et al. [5] and Pizzo et al. [6] attributed width effects to heat diffusion by sample sides. However, Mell et al. [4] hypothesized that these phenomena were caused by the convective heat transfer variation due to a change in width. Sidewall effects on upward flame spread across PMMA were explored by Tsai [7]. They observed that flames were higher and heat feedback was generally less when sidewalls were present. Thus, the effect of sidewalls lead to an increase in flame spread rates for narrow samples but a decrease for wide samples.

To date, the characteristics of XPS flame spread have not been sufficiently studied. There appears to be little consensus on the width effect and the mechanism involved. Furthermore, few researchers have focused on the effects of sample width and sidewalls on downward flame spread over XPS slabs. Therefore, this topic merits in-depth study.

In this work, a series of laboratory-scale experiments investigating downward flame spread over XPS were conducted. The flame spread characteristics of different sample widths and structures (with or without sidewalls) were compared. Furthermore, the effects of sample width and sidewalls on XPS flame spread behaviours were identified.

EXPERIMENTAL APPARATUS AND METHODS

As shown in Fig. 2, the experimental system is composed of a gypsum board, XPS sample, digital camera, computer, thermocouples, data collector and electronic balance. To insulate the heat generated during

combustion, a gypsum board was placed behind the sample. A digital camera, whose operating speed is 25 frames per second, was used to record the dynamic process of flame spread. When sidewalls were absent, two cameras were employed. Their positions are shown in Fig. 2(c). When sidewalls were present, only the front camera was used. The characteristic parameters of flame shape and flame front position were obtained through video processing in the computer. K-type thermocouples were used to obtain temperature data. The diameter and response time of thermocouples are 0.5mm and 0.03s, respectively. The measurement range of the thermocouples is -200-1200°C and their accuracy rating is 2.2°C. The probes of one set of thermocouples (number of thermocouples: 6) were inserted into the sample close to the upper surface to record surface temperature. The distribution of these thermocouples is given in Fig. 2(d). The other set (number of thermocouples: 2) was inserted into the sample to measure solid-phase temperature. The distance from these thermocouples to the upper surface was 2 cm. Both solid-phase thermocouples were positioned along the central axis of the sample, and their heights were the same as those of surface thermocouples. An electronic balance with precision of 0.01g was used to record sample mass change over time.

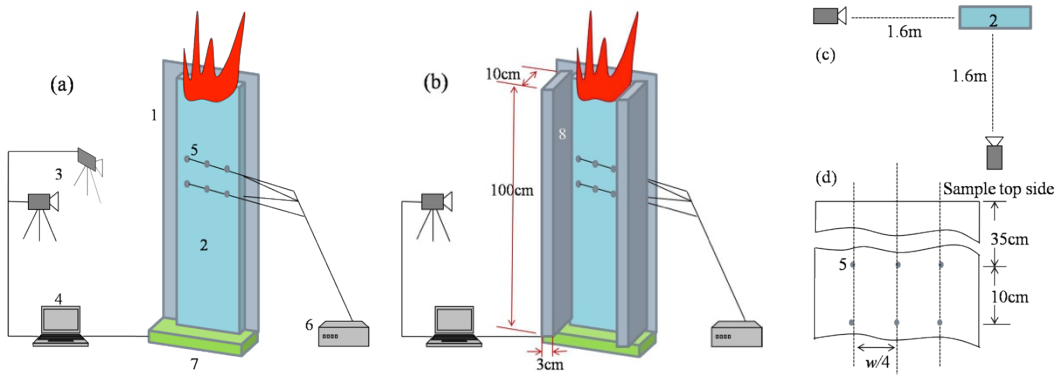

Fig. 2. Schematic illustration of the experimental system. (a) without sidewalls; (b) with sidewalls; (c) top view of cameras; and (d) distribution of thermocouples. 1. gypsum board; 2. XPS sample; 3. digital camera; 4. computer; 5. thermocouples; 6. data collector; 7. electronic balance; and 8. sidewalls.

The properties of the XPS samples are listed in Table 1. The sample widths tested were 4 cm, 8 cm, 12 cm and 16 cm. The experiments were conducted employing vertical samples with and without sidewalls. The edges of samples without sidewalls were left exposed. Where employed, sidewalls were made of foam glass, which exhibits good heat resistance and heat-shielding performance. The width, height and thickness of sidewalls were 10 cm, 100 cm and 3 cm, respectively. A linear igniter was employed to ignite the top portion of the sample. Each test was repeated three times under the same conditions to minimize experimental error.

Table 1. Properties of XPS samples.

Material	Density (kg/ m^3)	Length (cm)	Thickness (cm)	Specific heat (J/kg K)	Conductivity (W/m K)	Ignition temperature (K)
XPS	34.034	100	3	1400	0.028	628

EFFECTS OF SAMPLE WIDTH

Flame Shape

Figures 3(a) and (b) show the front view of the flame shape at different widths, with and without sidewalls. Flame height and flame area differed according to the circumstances. For all samples, the flame shape became more irregular with a rise in sample width. This demonstrates that air entrainment during flame spread is fiercer among wider samples. Where sidewalls were employed, the maximum flame height was observed beside the sidewalls. A similar phenomenon was described in Tsai's work [7].

The side view of the flame shape is shown in Fig. 3(c). The combustion zone was observed to be comprised of two parts: surface flame and adherence flame. The surface flame was formed due to the combustion of

pyrolysis gas of a sample cross-section. During flame spread, some molten XPS was left behind, and this attached to the gypsum board creating the adherence flame. Average maximum flame height (H) and average flame area (A), which are the most important characteristics of flame shape, will be discussed in the following sections.

Fig. 4 shows the flame front shape. Since the flame spread is downward, the angle between the flame surface and sample surface was large. Thus the radiative heat transfer from the flame to the sample surface was small. Most of the radiative heat was transferred to the sample cross-section. Therefore, it was apparent that under both conditions (with and without sidewalls), the flame spread over sample cross-section and the burning area was approximately equal to the cross-section area. Overall, it was considered that at the flame front, the burning area or burning width with sidewalls was approximately the same as that without sidewalls.

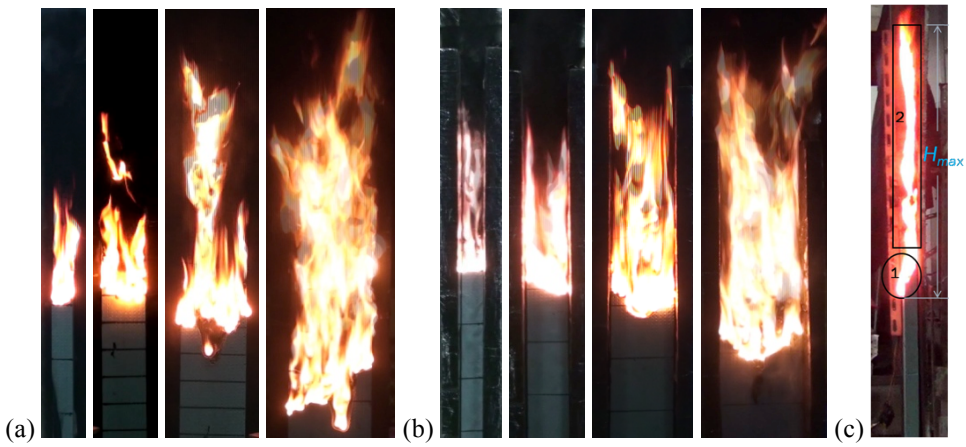

Fig. 3. Flame shapes at different widths. (a) without sidewalls; (b) with sidewalls; and (c) side view:1.surface flame; 2.adherence flame.

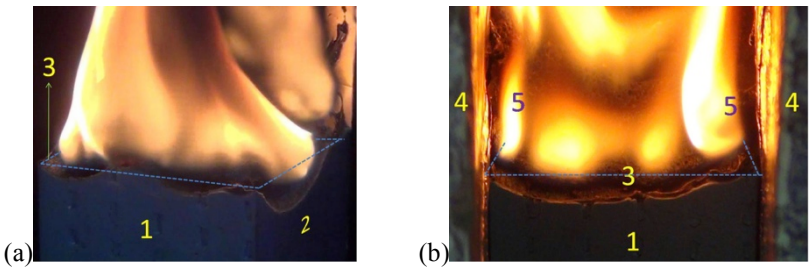

Fig. 4. Flame front shape (sample width: 4 cm). (a) without sidewalls; (b) with sidewalls. 1.sample front surface; 2.sample side surface; 3. cross section; 4.sidewall; 5. flame along the sample thickness.

Average Maximum Flame Height (*H*)

Maximum flame height (H_{max}) is defined as the maximum vertical distance between a flame tip and flame front. Flame images were recorded by the camera, and an appropriate threshold value of luminosity was set to determine flame contour. H_{max} was then obtained from the flame contour. Since H_{max} fluctuated with time, the concept of average maximum flame height (H), which is defined as the 50% flame tip appearance rate, is introduced in this study.

The results are presented in Fig. 5.

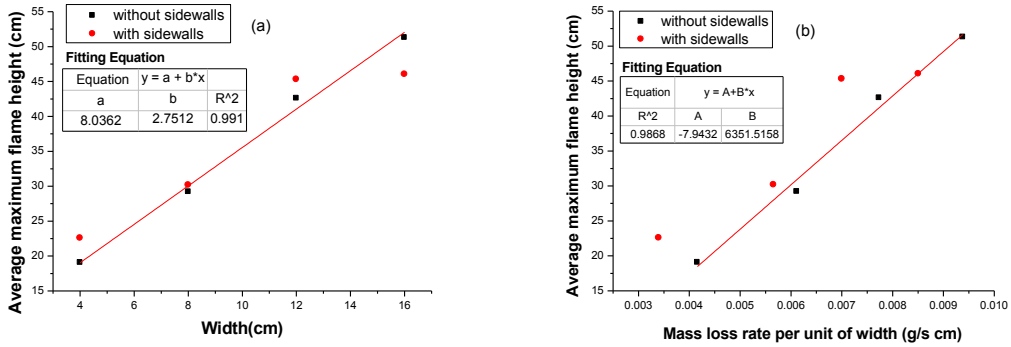

Fig. 5. Variation of average maximum flame height with width (a) and mass loss rate per unit of width (b).

As described in Fig. 5, H rises with an increase in sample width (w), regardless of the presence or absence of sidewalls. The phenomenon may be attributed to the increase in mass loss rate as the sample width rises. Higher mass loss rate leads to the release of additional pyrolysis gas. More air is needed, assuming that combustion is complete. Thus, the gas mixture volume is larger, causing greater flame volume and consequently higher flame height. The average values of mass loss rate per unit of width ($\dot{m}/W$) are listed in Table 2. W denotes the burning width, which should include the width of sample sides. Table 2 shows that $\dot{m}/W$ increases with a rise in sample width under both conditions tested. The experimental data verifies the above hypothesis.

Table 2. The absolute value of average mass loss rate per unit of width (g/s cm) under different conditions.

width	4cm	8cm	12cm	16cm
without sidewalls	0.00415	0.00614	0.00771	0.00941
with sidewalls	0.00338	0.00564	0.00699	0.00848

A linear relationship of H and w was found for samples without sidewalls, as shown in Fig. 5(a). Through curve fitting, it was established that the average maximum flame height also followed a linear function of mass loss rate per unit of width (Fig. 5(b)). The relationship differs from that of upward flame spread. The flame height for upward flame spread may be predicted from Eq. 1 [8-12], which suggests that the H is a function of $\dot{m}/W$ and can be represented by the following power law function,

$$H = a(\dot{m}h_c / W\rho_\infty c_p T_\infty \sqrt{g})^{2/3}. \quad (1)$$

However, the data acquired from experiments with sidewalls did not conform to the relationships above.

Average Flame Area

Flame area was obtained from images captured by the digital camera in front of the samples. Since flame area also fluctuated with time, the concept of average flame area (A) is introduced in this work. The average flame area was divided by the sample width to conduct an effective comparison. The results are shown in Fig. 6.

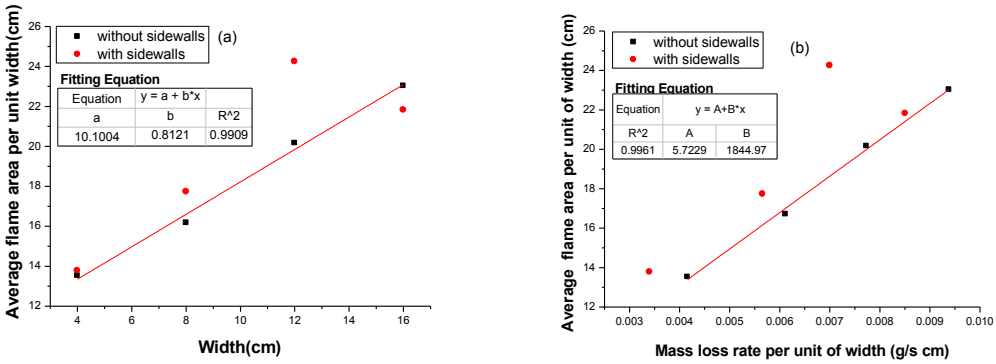

Fig. 6. Change of A/w with width (a) and mass loss rate per unit of width (b).

For samples without sidewalls, the variation in A/w with width and mass loss rate per unit width resemble those of H. It was also found that A/w followed a linear function of w and $\dot{m}/W$. When sidewalls were present, A/w first rose and then fell with an increase in width and mass loss rate per unit width.

Flame Spread Rate

Flame spread rate is defined as the propagation speed of a flame front relative to sample surface. The flame front position was obtained by processing the camera image sequences. To avoid the influence of ignition, the study was initiated after flames had spread a distance of 10 cm. Pool fires eventually formed on the floor, and influenced downward flame spread. To avoid this effect, every test was terminated when the flame spread distance reached 70 cm. The experimental data concerning flame front position as a function of time are shown in Fig. 7.

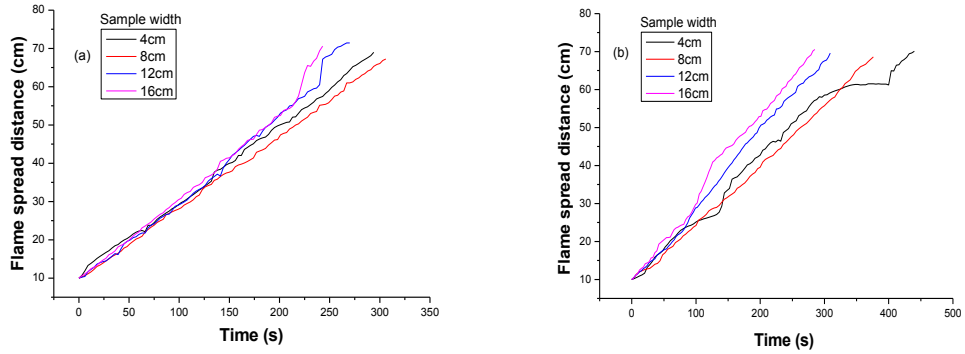

Fig. 7. Flame spread distance versus time (a) without sidewalls and (b) with sidewalls.

For samples without sidewalls, it was evident that the flame spread distance of the narrow samples (4 cm and 8 cm) increased linearly with time, although a few slight accelerations could be observed. In general, the flame spread rate was approximately constant for narrow samples. As the sample width was increased,, a linear increase in the flame spread was observed followed by significant acceleration, which demonstrates that the flame spread rate rose at the end of the spread process. The increase in flame spread rate may be attributed to the downward flow of molten materials. When drops of burning molten materials flowed downward, the unburned XPS between the flame front and burning drops was subject to greater heat flux. The unburned XPS was more rapidly ignited, and thus the flame front moved forward at an increasing speed. Moreover, the heat conduction from the molten XPS drops to unburned material could also promote flame spread.

For samples with sidewalls, deceleration and stagnation of flame spread could be observed with a sample width of 4 cm. For 8 cm and 12 cm wide samples, the flame spread rate did not change significantly with time. When the sample width reached 16 cm, flame spread acceleration was apparent, which may also have resulted from the downward flow of molten materials.

Through the calculation of change in the flame spread distance, the flame spread rate was obtained. This rate was not constant under certain conditions. In such cases, the flame spread rate was averaged for further analysis. The results are shown in Fig. 8.

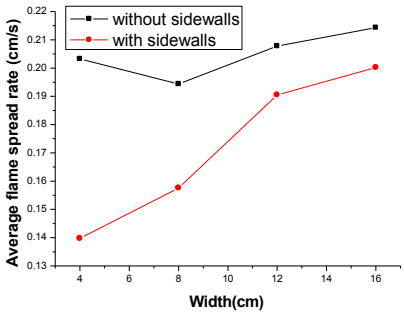

Fig. 8. Average flame spread rate under different conditions.

When sidewalls are absent, flame spread rate is seen in Fig. 8 to first drop and then rise with an increase in width (described as Trend I). However, the variation is not significant. When sidewalls are present, flame spread rate increases with a rise in width and the increase rate is large (described as Trend II).

Trend I may be explained by the theory of heat transfer. The flame spread rate is determined from the heat transfer from the combustion zone to the unburned materials. The heat transfer is comprised of two main elements: solid-phase heat conduction ($\dot{q}''_{cond}$) and gas-phase heat flux ($\dot{q}''_{g}$), as shown in Fig. 9. Zhang et al. [13] suggested that, since the heat-insulating property of XPS is good, solid-phase heat conduction through XPS is very small. However, the heat conductivity of molten XPS is much larger than that of XPS. Therefore, solid-phase heat conduction should not be ignored. The solid-phase heat conduction occurred near the gypsum board where the molten XPS accumulated.

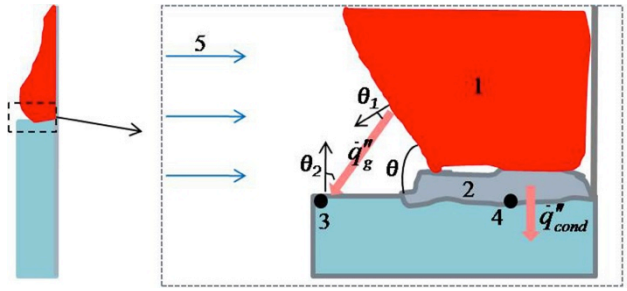

Fig. 9. Heat transfer process in flame spread. 1. flame; 2. molten XPS; 3. surface thermocouple; 4. solid-phase thermocouple; 5. front air flow.

The preheating length, which is the heat extension over the new material about to ignite, was acquired from the surface temperature gradient using Eq. 2 [14].

$$\delta_{ph} = \frac{T_{ig} - T_{\infty}}{|\, dT_s / dx \,|_{\max}} . \tag{2}$$

This equation was established for flames from burning thermally thin materials, whose heat flux transfers to unburned material mainly through the gas phase. Thus, the preheating length is positively correlated with gas-phase heat transfer. For thermally thick materials, dT_s/dx is also primarily determined from gas-phase heat transfer because T_s was measured employing the surface thermocouples which were scarcely affected by solid-heat transfer. Thus δ_{ph} obtained using Eq. 2 is still positively correlated with gas-phase heat transfer. The purpose of calculating δ_{ph} is to identify the changing trend of gas-phase heat transfer with an increase in sample width. Typical surface and solid-phase temperature curves are presented in Fig. 10(a). A first order derivative of the temperature was used to acquire the temperature gradient. Utilizing the surface

temperature gradient, δ_{ph} was obtained. Since there were six surface thermocouples in the experiment, values of δ_{ph} were averaged and are plotted in Fig. 10(b).

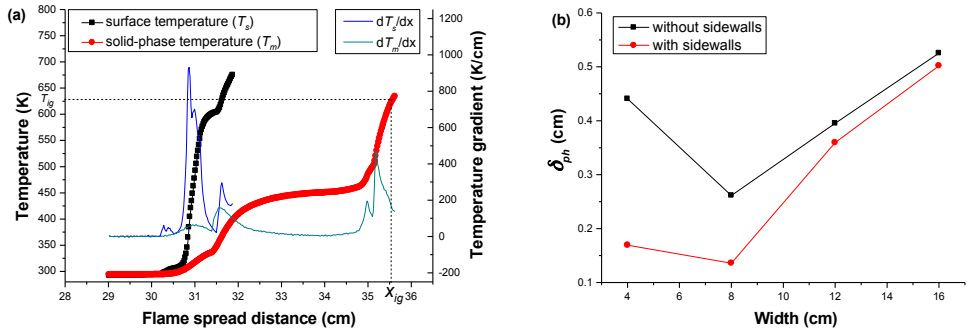

Fig. 10. (a) Recorded temperatures and their gradients versus flame spread distance (sample width: 4 cm, without sidewalls); (b) variation of δ_{ph} with width.

From Fig. 10(b), it may be observed that the preheating length first drops and then rises with an increase in width. Thus, the gas-phase heat transfer may have the same trend, which corresponds to Trend I. This suggests that heat transfer through the gas may determine the flame spread rate. This conclusion is consistent with the results of Chen et al. [15] and Blasi [16] who both demonstrated that for thermally thick materials, although the contribution of solid-phase heat conduction to the total energy transfer increased with the rise in fuel thickness, the gas-phase heat transfer was still dominant.

Solid-phase heat conduction could also have influenced flame spread rate, although it was not the decisive factor. The heat flux in the solid was obtained from Eq. 3.

$$\dot{q}''_{cond} = \lambda_m \left.\frac{\partial T_m}{\partial x}\right|_{x=x_{ig}} \tag{3}$$

where x_{ig} denotes the flame spread distance when the thermocouple in the solid reaches the ignition temperature. Employing the solid-phase temperature gradient, $\dot{q}''_{cond}$ was acquired. These values are presented in Table 3.

Table 3. Solid-phase heat flux at different widths.

Width	4cm	8cm	12cm	16cm
without sidewalls	$143.05\lambda_m$	$158.74\lambda_m$	$144.58\lambda_m$	$138.15\lambda_m$
with sidewalls	$94.26\lambda_m$	$112.20\lambda_m$	$127.14\lambda_m$	$132.84\lambda_m$

Solid-phase heat conduction is seen in Table 3 to first rise and then drop with an increase in width, which is inverse to the gas-phase heat transfer trend. The effects of the changing trend of solid-phase heat conduction with width counteract those of gas-phase heat transfer to a certain extent. Therefore, the variation in overall heat transfer and flame spread rate is not significantly affected by the width.

When sidewalls are present, the preheating length variation trend is not consistent with Trend II (Fig. 10(b)), which suggests that the gas-phase heat transfer is no longer the dominant factor. However, as is apparent from Table 3, Trend II corresponds with the solid-phase heat conduction trend. Thus, solid-phase heat conduction may determine flame spread rate with sidewalls.

In addition, the downward flow of molten XPS may also account for the larger v_f of wider samples. As described above, for some samples (width of 16 cm) with and without (widths of 12 cm and 16 cm) sidewalls, flame spread accelerations were observed due to the downward flow of molten material. This could have increased the average flame spread rate.

EFFECTS OF SIDEWALLS

The sidewall effects may be summarized as follows:

Effect I: The presence of sidewalls restricts air entrainment by the sample sides. Pyrolysis gas and oxygen could not mix sufficiently, causing insufficient oxygen for the pyrolysis gas near the sidewalls and gypsum board. Thus, the combustion of the sample with sidewalls was less effective than that without sidewalls. This agrees with Tsai's conclusion [7]. Moreover, Beaulieu and Dembsey [17] suggested that both flame convective heat flux and flame radiative heat flux decrease when the oxygen concentration is low. This may explain why gas-phase heat transfer is not the decisive factor in flame spread with sidewalls.

Effect II: Sidewalls change the flow orientation of convective air. The flow orientations with and without sidewalls are shown in Fig. 11. Since air entrainment by sample sides is restricted, the upward air flow is intensified (Fig. 11(a)). Furthermore, the sidewall effect is similar to the stack effect, which can promote upward air flow due to the difference in pressure between the top and bottom of the sample. Since the sidewall width is constant, a more narrow sample causes less air flow to be induced from the sample sides and higher upward air flow velocity. Williams [18] concluded that a dimensionless flame height follows Eq. 4:

$$\frac{H}{w} \propto \frac{u_0 w}{D_e}. \tag{4}$$

Upward air flow can increase the initial velocity of gaseous fuel (u_0). Thus, flame height increases as described by Eq. 4.

Effect III: As shown in Fig. 11(b), since side air entrainment is limited, the front air flow vertical to the sample surface is also intensified, assuming that the total volume of air entrainment is constant. Most of the pyrolysis gas from the cross section is pushed by the front air flow to the gypsum board. Thus the surface flame, which is an important factor influencing flame spread [19], is weakened. Furthermore, the surface flame angle θ becomes larger under the effect of front air flow (Fig. 9). The flame radiant heat flux may be obtained from Eq. 5 and Eq. 6 [20]:

$$\dot{q}'' = \varepsilon_f \sigma T_f^4 F_{12}, \tag{5}$$

$$F_{12} = \frac{1}{A_1}\int_{A_1}\int_{A_2} \frac{\cos\theta_1 \cos\theta_2}{\pi R^2} dA_1 dA_2 . \tag{6}$$

Radiant heat flux is significantly influenced by the view factor (F_{12}). Figure 9 depicts the mechanism by which θ_1 and θ_2 rise with an increase in flame angle θ, leading to a decrease in F_{12}. Thus, flame radiant heat flux falls under the effect of front air flow. Weaker surface flame and lower radiant heat flux lead to a shorter preheating length, as confirmed by Fig. 10(b). Since the primary source of gas-phase heat transfer is the surface flame, the weaker surface flame here may also account for the fact that gas-phase heat transfer is no longer the dominant factor in flame spread with sidewalls.

Effect IV: The adherence flame is driven closer to the molten XPS attaching to the gypsum board by the magnified front air flow. Thus, the molten XPS obtains additional heat flux from the flame, which leads to more complete combustion. Moreover, the stretched flame can ignite a greater area of molten material on the gypsum board. Therefore, less molten material is accumulated and flows downward. As discussed above, solid-phase heat conduction occurs primarily through molten materials. Hence, heat transfer through the solid phase with sidewalls is less than that without sidewalls, as is demonstrated in Table 3.

In addition, since sidewall width is invariable, the sidewall effects may be not significant for wide samples. The reason was hypothesized to be that considerable restriction of side air entrainment would occur. However, some air is induced from the sides to the combustion zone of wide samples (Fig. 11(b).3). Thus, the sidewall effects become less significant. It is speculated that sidewall effects are less considerable for narrower sidewalls. This is consistent with the conclusion of Yan *et al.* [21], who also found that when the sidewall width rose to a certain value, sidewall effects were slightly influenced by the increase in sidewall

width. In this paper, sidewall width was constant, and thus it was not possible to verify above deduction and conclusion. This work will be conducted in the future.

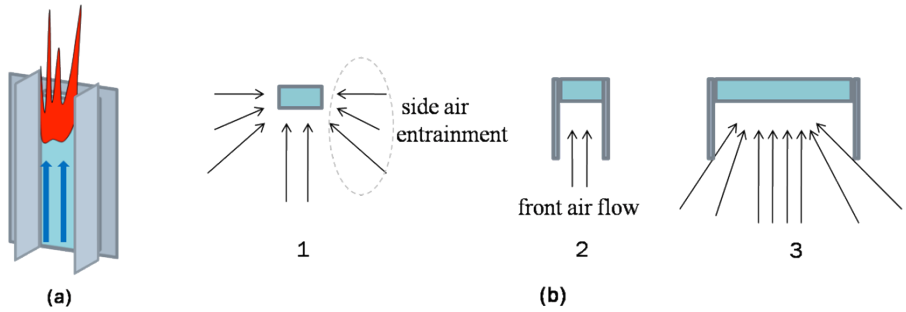

Fig. 11. Air flow orientation during flame spread. (a) side view; (b) top view: 1. sample without sidewalls; 2. narrow sample with sidewalls; 3. wide sample with sidewalls.

The four effects above were employed to interpret the following differences in experimental phenomena between samples with sidewalls and those without sidewalls.

Table 2 confirms that $\dot{m}$ with sidewalls is lower than that without sidewalls. The 'edge effect' and Sidewall Effects I, III may account for this phenomenon. When sidewalls were absent, samples edges were not blocked and the heat transfer to unburned zone may be more than that of samples whose sides were inhibited [22]. When sidewalls were present, Sidewall Effects I and III may reduce flame heat flux to unburned materials. The mass loss rate is primarily determined by the total heat transfer from flame to the unburned zone [23]. Thus $\dot{m}$ without sidewalls is higher.

From Fig. 5(a) it is evident that when the samples are narrow (4 cm, 8 cm, 12 cm), H with sidewalls is higher than that without sidewalls, while the reverse is true of wide samples (16 cm). These results differ from the conclusion reached by Tsai [7], who observed that the flame height with sidewalls was higher than that without sidewalls for all widths tested in his experiments (widths of 10 cm, 20 cm, 30 cm, 50 cm and 70 cm). The phenomenon observed in this work may be attributed to the interaction of Sidewall Effect II and the mass loss rate effect. For narrow samples, Sidewall Effect II is marked and more dominant than mass loss rate effect. Therefore H with sidewalls is higher. When the sample width increases to a certain value, Sidewall Effect II is weakened and the influence of $\dot{m}$ becomes more dominant. Thus, H without sidewalls is higher. In other words, when sidewalls are present, sample width (which is positively correlated with mass loss rate) is not the only factor determining flame height. Therefore, the relationship of H and w for samples with sidewalls is not linear. As seen in Fig. 6(a), A/w with sidewalls is higher than that without sidewalls for narrow samples, but lower for wide samples. A linear relationship does not exist between A/w and w for samples with sidewalls. The mechanism involved is similar to that outlined above in explaining the trend in H.

As shown in Fig. 7(b), deceleration and stagnation of flame spread occur at a sample width of 4 cm with sidewalls. Sidewall Effects I and III may account for this phenomenon. Both the convective heat flux and radiative heat flux of the surface flame decrease due to Sidewall Effect I. Sidewall Effect III could also weaken the surface flame. Huang et al. [19] demonstrated that surface flame influences flame spread rate significantly, while pool flame (similar to the adherence flame in this work) contributes little to spread rate. Therefore, flame spread deceleration was observed in this work. When the sample is narrow, Sidewall Effect I and III are marked. The unburned materials cannot acquire enough heat from the weak surface flame to sustain pyrolysis, which ultimately leads to quenching of the surface flame, and thus stagnates spread. However, it was observed that the adherence flame was not quenched. Heat flux from the adherence flame was transferred to the unburned materials. When the heat accumulated to a certain extent, the unburned XPS was reignited and flame spread continued.

From Fig. 7 it is apparent that flame spread acceleration with sidewalls occurred at larger widths than that without sidewalls. As discussed above, flame spread acceleration may have been caused by the downward flowing of molten materials. As discussed in Sidewall Effect IV, the molten XPS combustion was therefore more complete, and less molten material flowed downward. Thus, flame spread acceleration did not occur

in the 12 cm wide sample with sidewalls. For wider samples (16 cm), Effect IV becomes less significant. Therefore, flame spread acceleration was observed with and without sidewalls.

Fig. 8 demonstrates that flame spread rate without sidewalls is higher than that with sidewalls. This finding is different from Tsai's conclusion regarding upward flame spread across a PMMA surface [7]. This phenomenon may be attributed to sidewall effects and edge effects. As discussed above, Sidewall Effects I and III decrease flame heat flux to unburned materials. Sidewall Effect III weakens the surface flame. The molten XPS is reduced due to sidewall effect IV. The solid-phase heat conduction and gas-phase heat transfer for samples with sidewalls are smaller than those without sidewalls. All these effects account for the lower flame spread rate of samples with sidewalls. As for the edge effects, Comas and Pujol [24] found that the increase of oxygen supply along the free edge lead to a greater flame spread rate for samples with edges uninhibited. A computational study on opposed flow flame spread was conducted by Kumar and Kumar [22], who explored the 'edge effect' and suggested that increased heat transfer for free-side-burning fuel strips accounted for the higher spread rate, as compared to fuel strips with inhibited sides. In this work, the edges of samples without sidewalls were left exposed while samples with sidewalls inhibited their edges. Thus the edge effect leads to higher flame spread rate along samples without sidewalls. Moreover, when sidewalls were absent, the downward flow of molten XPS on sample sides may increase the spread rate, which is also considered an edge effect.

Mamourian et al. [25] used mass loss data to predict the downward flame spread distance of PMMA (Eq. 7):

$$Y = (m_0 - m) / (\rho . A_c). \tag{7}$$

The same method is employed in this work. Furthermore, the predicted flame spread rate may be obtained through Eq. 8:

$$v_p = dY / dt = -\frac{\dot{m}}{\rho A_c} \tag{8}$$

It was found that the predicted flame spread rate value was smaller than the measured value under all conditions. The reason for this deviation is that the speed of flame spread on the sample surface was higher than the forward velocity of the cross-section, leaving large quantities of molten XPS on the gypsum board. Moreover, the dropping of molten XPS may promote flame spread rate, but does not have a significant effect on mass loss rate. Therefore, the measured values were higher than those predicted. In addition, as adherence flames are much larger than surface flames (Fig. 3(c)), the mass loss rate is primarily determined by the combustion intensity of the adherence flame. However, flame spread rate is principally determined by the surface flame. Thus, no positive correlation between flame spread rate and mass loss rate was found in some cases. For instance, $\dot{m}$ of the 8 cm wide sample was larger than that of the 4 cm wide sample, whereas v_f of the 8 cm wide sample was smaller than that of the 4 cm wide sample.

Eq. 9 may be employed to estimate the mass of molten XPS generated per unit time. The estimated values under different conditions are listed in Table 4.

$$\dot{m}_1 = \rho A_c (v_f - v_p) \tag{9}$$

From Table 4, it is evident that the mass growth rate of molten XPS for samples without sidewalls was larger than that with sidewalls, which confirms our analysis of Sidewall Effect IV.

Table 4. Estimation of molten XPS mass growth rate (g/s) under different conditions.

width	4 cm	8 cm	12 cm	16 cm
without sidewalls	0.0359	0.0623	0.0988	0.1195
with sidewalls	0.0194	0.0412	0.0919	0.1187

CONCLUSIONS

The effects of sample width and sidewalls on the characteristics of flame spread over XPS slabs were investigated in this work. A series of laboratory-scale experiments were conducted and the spread processes were recorded. Furthermore, the maximum flame height, flame area, flame spread rate, mass loss rate, preheating length and molten XPS mass growth rate were obtained. The influences of width and sidewalls on these flame spread characteristics were analyzed. The results of the study are summarized as follows:

(1) For XPS without sidewalls, the average maximum flame height (H) and average flame area per unit width (A/w) rises linearly with an increase in sample width (w) and mass loss rate per unit of width. For XPS with sidewalls, a rise in sample width and mass loss rate causes H to increase, while A/w to first increase and then decrease.

(2) When sidewalls are absent, the flame spread rate first decreases and then rises with an increase in width. This trend is determined by gas-phase heat transfer. When sidewalls are present, flame spread rate increases with a rise in width, and solid-phase heat conduction determines the trend.

(3) Effects of sidewalls included : low oxygen concentration near the sidewalls and gypsum board, which leads to lower flame heat flux; upward and front air flow are intensified; the flame is stretched and the surface flame is weakened; molten XPS mass decreases. Sidewall effects are significant for narrow samples.

(4) For narrow samples, H and A/w with sidewalls are higher than those without sidewalls, while the reverse is true of wider samples. The mass loss rate, preheating length and average flame spread rate with sidewalls are smaller than those without sidewalls.

(5) Deceleration and stagnation of flame spread occur at a sample width of 4 cm with sidewalls. Flame spread acceleration with sidewalls occurs at a greater width than that without sidewalls.

ACKNOWLEDGEMENTS

This research is supported by the National Basic Research Program of China (973 Program, Grant. No. 2012CB719702), the Research Fund for the Doctoral Program of Higher Education (NO. 20113402110023), the National Natural Science Foundation of China (No. 50976110 and No. 51206002) and the Key Technologies R&D Program of China during the 12th Five-Year Plan Period (No. 2013BAJ01B05). The assistance from the Young Teacher Fund (No. QZ201109) of Anhui University of Technology and the open fund of the State Key Laboratory of Fire Science (No. HZ2012-KF04 and No. HZ2012-KF08) are also appreciated.

REFERENCES

[1] Zhang, Y., Huang, X.J., Wang, Q.S., Ji, J., Sun, J.H. and Yin, Y., (2011) Experimental study on the characteristics of horizontal flame spread over XPS surface on plateau, Journal of Hazardous Materials 189: 34-39, http://dx.doi.org/10.1016/j.jhazmat.2011.01.101

[2] Huang, X.J., Sun, J.H., JI, J., Zhang, Y., Wang, Q.S. and Zhang, Y., (2011) Flame spread over the surface of thermal insulation materials in different environments, Chinese Science Bulletin 56: 1617-1622, http://dx.doi.org/10.1007/s11434-010-4187-z

[3] Li, J., Ji, J., Zhang, Y. and Sun, J.H., (2009) Characteristics of flame spread over the surface of charring solid combustibles at high altitude, Chinese Science Bulletin 54:1957-1961, http://dx.doi.org/10.1007/s11434-009-0272-6

[4] Mell, W. and Kashiwagi, T., "Dimensional effects on the transition from ignition to flame spread in microgravity," *Proceedings of the Combustion Institute*, Combustion Institute, 1998, pp.2635-2641.

[5] Rangwala, A., Buckley, S. and Torero, J., "Upward flame spread on a vertically oriented fuel surface: The effect of finite width," *Proceedings of the Combustion Institute*, Combustion Institute, 2007, pp.2607-2615.

[6] Pizzo, Y., Consalvi, J., Querre, P., Coutin, M. and Porterie, B., (2009) Width effects on the early stage of upward flame spread over PMMA slabs: Experimental observations, Fire Safety Journal 44: 407-414, http://dx.doi.org/10.1016/j.firesaf.2008.09.003

[7] Tsai, K., (2011) Influence of sidewalls on width effects of upward flame spread, Fire Safety Journal 46:294–304, http://dx.doi.org/10.1016/j.firesaf.2011.03.006

[8] Hasemi, Y., "Thermal Modeling of Upward Wall Flame Spread," *Fire Safety Science -- Proceedings of the first International Symposium*, International Association for Fire Safety Science, 1986, pp. 87-96.

[9] Quintiere, J., Harkleroad, M. and Hasemi, Y., (1986) Wall Flames and Implications of Upward Flame Spread, Combustion Science and Technology 48: 191-222, http://dx.doi.org/10.1080/00102208608923893

[10] Hasemi, Y., (1984) Experimental Wall Flame Heat Transfer Correlation for the Analysis of Upward Flame Spread, Fire Science and Technology 4:75-90, http://dx.doi.org/10.3210/fst.4.75

[11] Ahmad, T. and Faith, G.M., "Turbulent Wall Fire," *Proceedings of the Combustion Institute*, Combustion Institute, 1979, pp.1149-1160.

[12] Brehob, E.G. and Kulkarni, A.K., (1993) Time-dependent mass lass rate behavior of wall materials under external radiation, Fire and Materials 17:249-254, http://dx.doi.org/10.1002/fam.810170507

[13] Zhang, Y., Sun, J.H., Huang, X.J. and Chen, X.F., (2013) Heat transfer mechanisms in horizontal flame spread over wood and extruded polystyrene surfaces, International Journal of Heat and Mass Transfer 61: 28–34, http://dx.doi.org/10.1016/j.ijheatmasstransfer.2013.01.069

[14] Bhattacharjee, S., Altenkirch, R.A. and Sacksteder, K., (1996) The effect of ambient pressure on flame spread over thin cellulosic fuel in a quiescent microgravity environment, Journal of Heat Transfer 118:181-190, http://dx.doi.org/10.1115/1.2824032

[15] Chen, P., Sun, J.H. and He, X.C., (2007) Behavior of Flame Spread Downward over Thick Wood Sheets and Heat Transfer Analysis, Journal of Fire Sciences 25: 5-21, http://dx.doi.org/10.1177/0734904107062356

[16] Di Blasi, C., (1994) Processes of Flames Spreading over the Surface of Charring Fuels: Effects of the Solid Thickness, Combustion and Flame 97:225-239, http://dx.doi.org/10.1016/0010-2180(94)90006-X

[17] Beaulieu, P.A. and Dembsey, N.A., (2008) Effect of oxygen on flame flux in horizontal and vertical orientations, Fire Safety Journal 43: 410-428, http://dx.doi.org/10.1016/j.firesaf.2007.11.008

[18] Williams, F.A. *Combustion Theory*, Benjamin Cummings, Menlo Park, California, 1985, p.42.

[19] Huang, X., Wang, Q., Zhang, Y., Yin, Y. and Sun, J., (2012) Thickness effect on flame spread characteristics of expanded polystyrene in different environments, Journal of Thermoplastic Composite Materials 25: 427-438, http://dx.doi.org/10.1177/0892705711411341

[20] Incropera, F.P., DeWitt, D.P., Bergman, T.L. and Lavine, A.S., Fundamentals of Heat and Mass Transfer, Wiley, Hoboken, U.S., 2006, p.443.

[21] Yan W., Shen Y., An W., Zhou Y., Jiang L. and Sun J., Experimental Study on the Influence of the U-shape Wall on the Upward Flame Propagation of Insulation Material. Fire and Materials (submitted)

[22] Kumar C. and Kumar A., (2010) A Computational Study on Opposed Flow. Flame Spread Over Thin Solid Fuels with Side-Edge Burning, Combustion Science and Technology, 182:9, 1321-1340, http://dx.doi.org/10.1080/00102201003694842

[23] Fang J., Ran T., Guan J., Wang J. and Zhang Y., (2011) Influence of low air pressure on combustion characteristics and flame pulsation frequency of pool fires. Fuel 90: 2760–2766, http://dx.doi.org/10.1016/j.fuel.2011.03.035

[24] Comas B. and Pujol T., (2012) Experimental Study of the Effects of Side-Edge Burning in the Downward Flame Spread of Thin Solid Fuels, Combustion Science and Technology, 184:4, 489-504, http://dx.doi.org/10.1080/00102202.2011.648033

[25] Mamourian, M., Esfahani, J. A. and Ayani, M. B., (2009) Experimental Investigation of the Effect of the Solid Fuel Dimensions on the Downward Flame Spread, Kuwait Journal of Science & Engineering 36:183-200, http://profdoc.um.ac.ir/paper-abstract-1014075.html